Astronomy & Astrophysics manuscript no. 0088 © ESO 2008
July 30, 2008

arXiv:0806.1647v2 [astro-ph] 30 Jul 2008

The radio spectrum and magnetic field structure of SNR HB3

W. B. Shi[1,3], J. L. Han[1], X. Y. Gao[1], X. H. Sun[1], L. Xiao[1], P. Reich[2], and W. Reich[2]

[1] National Astronomical Observatories, Chinese Academy of Sciences, Jia 20 DaTun Road, ChaoYang District,
Beijing 100012, China
e-mail: `hjl@bao.ac.cn`
[2] Max-Planck-Institut für Radioastronomie, Auf dem Hügel 69, 53121 Bonn, Germany
[3] School of Space Science and Physics, Shandong University at Weihai, 180 Cultural West Road, Shandong 264209, China

Received 29 April 2008 / Accepted 7 June 2008

ABSTRACT

Context. Evidence for a spectral flattening of the supernova remnant (SNR) HB3 (G132.7+1.3) was recently claimed in literature based on previously published total flux density data, and the flattening was further interpreted as the discovery of thermal bremsstrahlung emission in the shell of HB3.
Aims. A spectral flattening has never been observed from any SNR before. Reliable observations of HB3 at frequencies above 3000 MHz are crucial to confirm such a spectral behaviour.
Methods. We extracted 4800 MHz total intensity and polarisation data of HB3 from the Sino-German 6 cm polarisation survey of the Galactic plane made with the Urumqi 25 m telescope, and analysed the spectrum of HB3, together with Effelsberg data at 1408 MHz and 2675 MHz.
Results. We found an overall spectral index of HB3 of $\alpha = -0.61 \pm 0.06$ between 1408 MHz and 4800 MHz, similar to the index at lower frequencies. There is no spectral flattening at high frequencies. We detected strong polarised emission from HB3 at 4800 MHz. Our 4800 MHz data show a tangential field orientation in the HB3 shell.

Key words. ISM: supernova remnant – ISM: individual: HB3 – radio continuum: ISM – HII regions

1. Introduction

Radio emission from a supernova remnant (SNR) originates from synchrotron emission of relativistic electrons gyrating in the enhanced magnetic fields in its shell or filaments. The observed radio spectrum of a SNR generally follows a power-law ($S_\nu \propto \nu^\alpha$, where α is the spectral index). A definite case of a spectral break was detected for the SNR S147 (Fürst & Reich, 1986; Xiao et al., 2008).

HB3 is a large ($1\overset{\circ}{.}5 \times 2^\circ$) and evolved SNR, with an age of about 30000 yr (Lazendic & Slane, 2006). It is located at the edge of the HII regions W3/W4 and belongs to a complex of molecular clouds, star-formation and HII regions (W3/W4/W5) (e.g., Digel et al., 1996) in the Perseus arm at a distance of about 2.2 kpc (Routledge et al., 1991; Xu et al., 2006). Although the SNR HB3 partly overlaps with the adjacent HII regions, W3/W4, in the low-resolution radio maps, signs of a real interaction, such as a deformed shell in the high-resolution maps or OH masers in the joint region from the HB3 shock, have not been detected (Koralesky et al., 1998; Kothes et al., 2006). Nevertheless, enhanced radio emission has been observed at all radio bands in the southeastern regions of HB3 (towards the lower-left in Fig. 1).

Previous estimates of the spectral index of HB3 were made from flux densities determined at frequencies up to 3 GHz, mostly without point source subtraction. The spectral index of HB3 was quoted to have values of $\alpha = -0.64 \pm 0.01$ (Fesen et al., 1995), $\alpha = -0.56 \pm 0.03$ (Green, 2007), $\alpha = -0.60 \pm 0.04$ (Landecker et al., 1987), and $\alpha = -0.66 \pm 0.02$ (Kothes et al., 2006). Flux-density estimates of HB3 from low-resolution observations are uncertain, especially at high frequencies, because of the partial overlap with W3/W4 (see Green, 2007).

Recently, Tian & Leahy (2005) obtained images of HB3 at 408 MHz and 1420 MHz from the Canadian Galactic Plane Survey (CGPS: Taylor et al., 2003) with compact sources and diffuse background emission subtracted. They derived a spectral index for HB3 of $\alpha = -0.34 \pm 0.25$ between these two frequencies (Tian & Leahy, 2005, 2006, erratum). This result was confirmed by the TT-plot method. They also found a surprising result: *a spectral flattening of the overall HB3 spectrum above 1 GHz*, derived from all published flux density data from 38 MHz to 3900 MHz. Urošević et al. (2007) fitted the spectrum using a two-component model of synchrotron emission and thermal bremsstrahlung emission. They and concluded that the flattening is evidence for the detection of thermal bremsstrahlung emission produced in the shell of the SNR. However, there are severe problems in the determination of flux density data of HB3, as discussed by Green (2007). The uncertainties in the quoted flux density data, especially at high frequencies (1 GHz to 3 GHz), are large, therefore the spectral flattening has been discredited by Green (2007). Radio observations at even higher frequencies are required to clarify this extraordinary spectral behaviour.

The ongoing *Sino-German λ6 cm polarisation survey of the Galactic plane* (Sun et al., 2007) has already covered the HB3 area. In this paper, we analyse our λ6 cm (4800 MHz) data together with 1408 MHz and 2675 MHz data from the Effelsberg Galactic plane surveys (Reich et al., 1997; Fürst et al., 1990a) to determine the high-frequency spectrum of HB3. Furthermore, instead of using radio emission of the entire SNR, where its eastern part obviously suffers from contamination or confusion by thermal emission, we limit our study to the part being almost

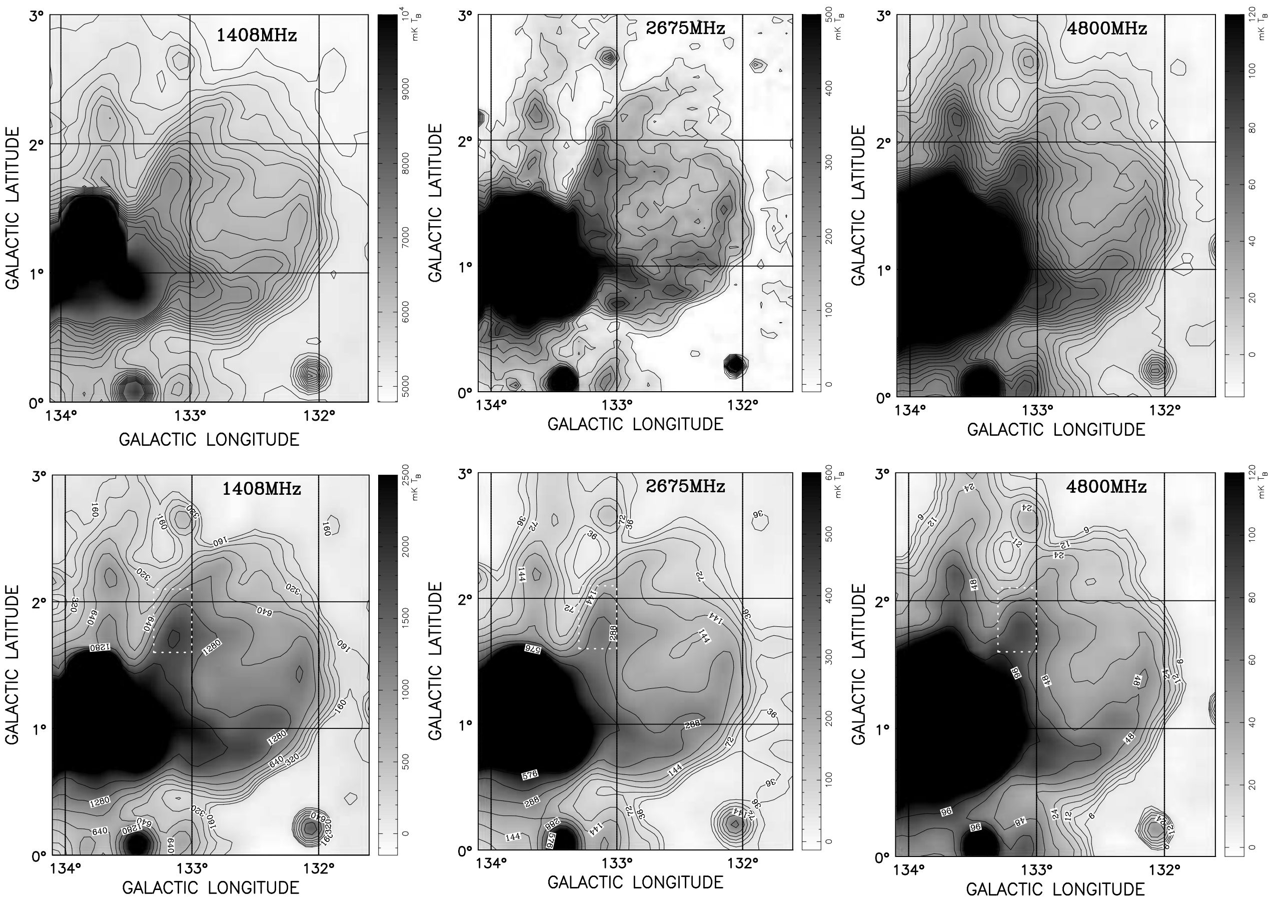

Fig. 1. HB3 maps at 1408 MHz, 2675 MHz, and 4800 MHz. The top row shows the data after the subtraction of point-like sources in the area of HB3 and $10'$ outside. The angular resolution at 1408 MHz, 2675 MHz, and 4800 MHz is $9\farcm4$, $4\farcm3$, and $9\farcm5$, respectively. The bottom row displays the same data convolved to a common angular resolution of $10'$.

free of distortions. The first detection of polarised emission of HB3 at λ6 cm will also be briefly discussed.

2. Radio data of the HB3 region

The 1408 MHz data are extracted from the Galactic plane survey[1] observed with the Effelsberg 100 m telescope (Reich et al., 1997). The 2675 MHz data were observed in 1998 in the same way as the early 11cm survey Fürst et al. (1990a) but with a better receiver and higher sensitivity. The angular resolutions are $9\farcm4$ and $4\farcm3$, respectively. The new 4800 MHz data were observed with the Urumqi 25 m radio telescope with an angular resolution of $9\farcm5$. Observations were made by scans over 10° in length in both Galactic longitude and latitude, which is the limiting size for a reliable flux density determination of an object. Technical details of the 4800 MHz observations and data processing are described by Sun et al. (2007).

For a more accurate determination of the radio emission of HB3 at these three frequencies, we first identified and then subtracted unresolved point sources above the local surrounding level of diffuse emission in the region of HB3 and $10'$ outside. In total, 107 point sources have been identified on the high-resolution CGPS maps at 408 MHz and 1420 MHz (Taylor et al., 2003), and their spectral indices were determined if visible at both frequencies. Their fluxes at 2675 MHz and 4800 MHz were obtained by extrapolation. However, the fluxes of seven compact sources at 2675 MHz have been taken from Fürst et al. (1990b) and of eight point-like sources at 4800 MHz from the 87GB catalogue of Gregory & Condon (1991). The resulting maps are shown in the upper part of Fig. 1.

Table 1. Spectral indices of the HB3 regions

Freq. pairs	$\alpha_{133\mathrm{west}}$	$\beta^{\mathrm{TT}}_{133\mathrm{west}}$	$\alpha_{\mathrm{east.box}}$	$\beta^{\mathrm{TT}}_{\mathrm{east.box}}$
1408/2675	-0.51 ± 0.16	-2.64 ± 0.09	-0.49 ± 0.25	-2.69 ± 0.02
1408/4800	-0.61 ± 0.06	-2.61 ± 0.05	-0.53 ± 0.09	-2.54 ± 0.16
2675/4800	-0.71 ± 0.18	-2.57 ± 0.20	-0.58 ± 0.28	-2.32 ± 0.10

The large-scale Galactic background/foreground emission is obviously not uniform in the maps. Clearly it is stronger in the eastern part than in the western part, and stronger in the south than in the north. We subtracted a “twisted” base-level, so that the intensity level of the area surrounding HB3 is close to zero, hence, removed the large-scale Galactic emission. We then convolved all maps to the same $10'$ angular resolution for the spectral index analysis.

3. Spectral analysis of HB3

The boundary between HB3 and the adjacent HII regions can be fairly well defined in high-resolution low-frequency maps (Green, 2007), but this is difficult for our low-resolution maps. To avoid the contamination problem that Green (2007) emphasised, the HB3 region west of $l = 133^\circ$ and in an eastern box

---

[1] http://www.mpifr.de/survey.html

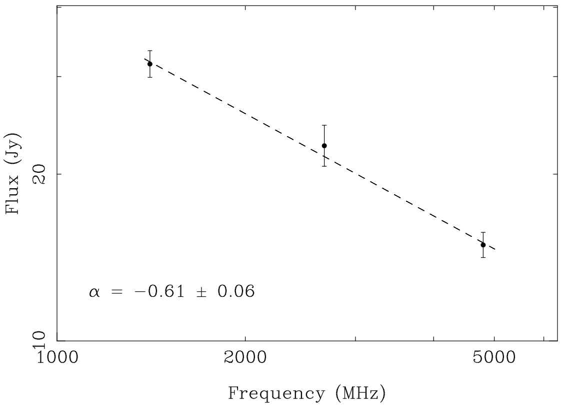

Fig. 2. Spectrum of the HB3 region west of $l = 133°$.

region (defined as $l = 133°$ to $133\overset{\circ}{.}3$, $b = 1\overset{\circ}{.}6$ to $2\overset{\circ}{.}1$) are analysed quantitatively. No contamination from W3/W4 appears in these regions for all three frequencies (see Fig. 1).

Fig. 2 shows that the integrated flux densities of the HB3 region west of $l = 133°$ decrease with frequency. The spectral index between 1408 MHz and 4800 MHz is $\alpha \sim -0.6$, consistent with the value Landecker et al. (1987) obtained from 408 MHz and 1420 MHz maps, and that from the low-frequency integrated flux densities in Kothes et al. (2006) and in Fig.3 of Tian & Leahy (2005).

The HB3 spectral behaviour can be verified by the so called TT-plot method (see Fig. 3), which largely reduces the influence of unrelated large-scale emission. Having convolved the maps to the same angular resolution, the pixel values at every $5'$ sampling for a selected area are plotted against each other. The slope β determined by linear regression is the brightness temperature spectral index ($T \propto \nu^{\beta}$). The flux density spectral index, α, is related to β as $\beta = \alpha - 2$. The α and β values in Figs. 2 and 3 are consistent (see Table 1). The emission in the eastern box region has a spectral behaviour similar to the HB3 region west of $l = 133°$.

The basic assumption for a reliable TT-plot method is that the emission at each pixel of the extended object has the same spectral index between the two frequencies, though the intensity varies from pixel to pixel. This is the case for many SNRs, but is not always true. Deviations from the fitted slope of a TT-plot may indicate either a possible spectral deviation for a certain region or base-level fluctuations across the object. In Fig. 4, we show the resolved spectral index maps. The very central part of HB3 seems to have a steeper spectrum, although the low intensity there also implies a larger uncertainty in the spectral index.

4. Polarised radio emission

From our 4800 MHz observations, we clearly detected polarised emission from HB3 for the first time (see Fig. 5). No polarised emission has been detected at lower frequencies, so Faraday rotation of the polarisation angles cannot be corrected. The polarised emission of HB3 at 4800 MHz is strongest in the eastern shell with a percentage polarisation of up to 28%. Some large-scale, polarised diffuse Galactic foreground emission is also visible in the map.

Pulsar rotation measures in the direction of the Perseus arm are a few tens of rad m^{-2} at maximum (Han et al., 1999). This results in a polarisation angle rotation of less than $20°$ at 4800 MHz. A $90°$ rotation of our observed $\boldsymbol{E}$ vectors roughly indicates the magnetic field orientation. Magnetic field lines seem to follow the shell, including the weak polarised emission in the western limb, which is a typical characteristic of an evolved SNR. A very exceptional area showing a radial magnetic field is located in the extreme southern part of the rim. It resembles a circular half shell with a diameter of $20'$, centred at $(l, b) = (132\overset{\circ}{.}75, 0\overset{\circ}{.}55)$ (see *the right panel* of Fig. 5, and also the Hα image, Fig. 8, of Fesen et al. 1995). Based on the distinct magnetic morphology, we suspect this may be another young SNR, rather than a limb of HB3. However, higher-resolution polarisation observations are needed to clarify the nature of this feature.

In the central region, where complete depolarisation occurs in our 4800 MHz map, ring-like X-ray emission has been detected by the Einstein satellite (for a comparison with the radio emission see Landecker et al., 1987; Venkatesan et al., 1984) and more recent ROSAT observations (see Fig.11 in Lazendic & Slane, 2006).

5. Discussion and Conclusions

We studied the spectrum of HB3 using maps at 1408 MHz, 2675 MHz, and 4800 MHz for the regions of HB3 where no contamination from W3/W4 is visible. We obtained a spectral index for HB3 between 1408 MHz and 4800 MHz of $\alpha = -0.61 \pm 0.06$, which is consistent with values obtained by Fesen et al. (1995), Landecker et al. (1987), Kothes et al. (2006). The TT-plot method was used to verify the spectrum. The new 4800 MHz data directly show that the spectrum of HB3 is constant with $\alpha \sim -0.6$ from 1 GHz to 5 GHz. There is no evidence for a spectral flattening to higher frequencies discussed earlier by Tian & Leahy (2005). This conclusion is in entire agreement with Green (2007). Therefore, the thermal bremsstrahlung emission discussed by Urošević et al. (2007) does not exist in the HB3 areas not contaminated by thermal emission related to W3/W4.

Polarised radio emission is clearly detected, which indicates that the magnetic field is aligned with the shell of HB3, except for the southern spherical limb, which we suspect to be an independent feature.

Acknowledgements. The λ6 cm data were obtained with the receiver system from the MPIfR mounted at the Nanshan 25 m telescope at the Urumqi Observatory of NAOC. The authors are supported by the National Natural Science Foundation (NNSF) of China (10521001 and 10773016), the National Key Basic Research Science Foundation of China (2007CB815403), and the Partner group of the MPIfR at NAOC in the frame of the exchange program between MPG and CAS for many bilateral visits. We thank Dr. James Anderson for carefully reading the manuscript.

References

Digel, S. W., Lyder, D. A., Philbrick, A. J., Puche, D., & Thaddeus, P. 1996, ApJ, 458, 561
Fesen, R. A., Downes, R. A., Wallace, D., & Normandeau, M. 1995, AJ, 110, 2876
Fürst, E., & Reich, W. 1986, A&A, 163, 185
Fürst, E., Reich, W., Reich, P., & Reif, K. 1990a, A&AS, 85, 691
Fürst, E., Reich, W., Reich, P., & Reif, K. 1990b, A&AS, 85, 805
Green, D. A. 2007, Bulletin of the Astronomical Society of India, 35, 77
Gregory, P. C. & Condon, J. J. 1991, ApJS, 75, 1011
Han, J. L., Manchester, R. N., & Qiao, G. J. 1999, MNRAS, 306, 371
Koralesky, B., Frail, D. A., Goss, W. M., Claussen, M. J., & Green, A. J. 1998, AJ, 116, 1323
Kothes, R., Fedotov, K., Foster, T. J., & Uyanıker, B. 2006, A&A, 457, 1081
Landecker, T. L., Vaneldik, J. F., Dewdney, P. E., & Routledge, D. 1987, AJ, 94, 111
Lazendic, J. S., & Slane, P. O. 2006, ApJ, 647, 350
Reich, P., Reich, W., & Fürst, E. 1997, A&AS, 126, 413

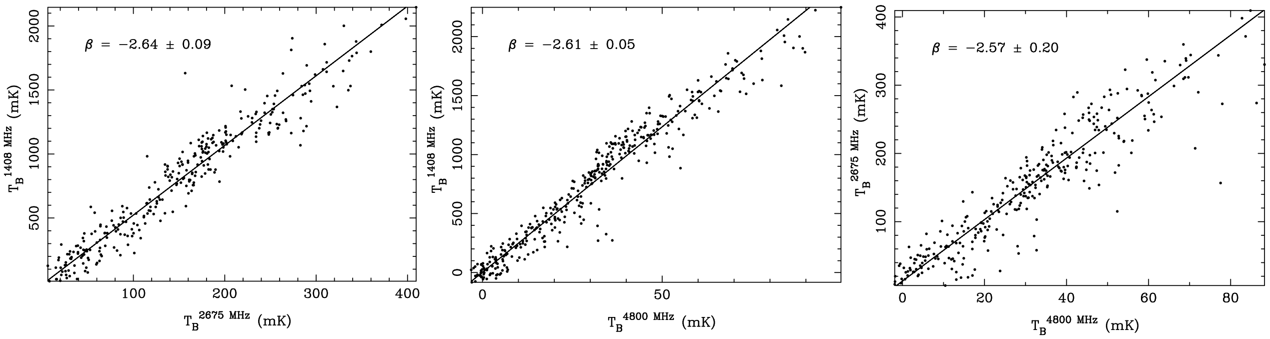

Fig. 3. TT-plots of the HB3 region west of $l = 133°$.

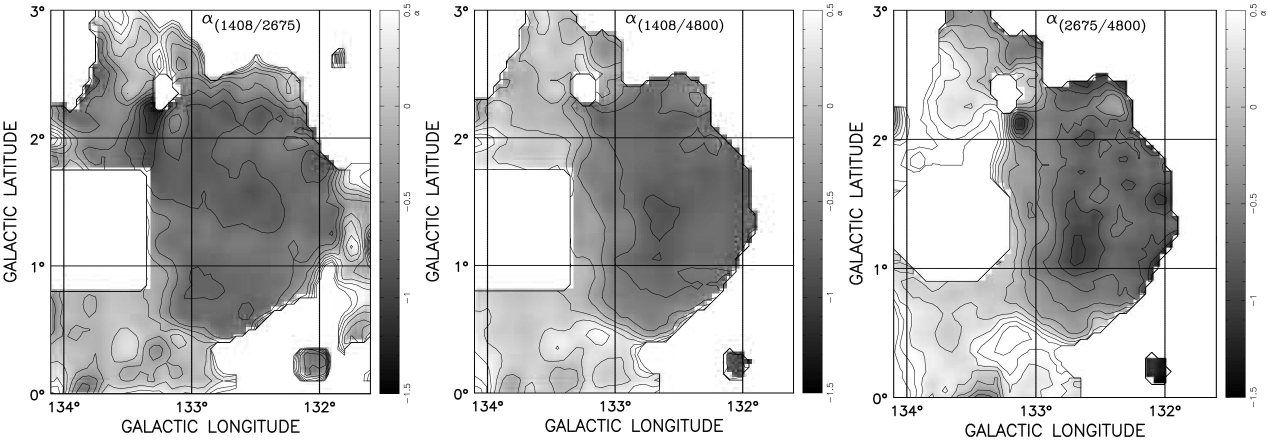

Fig. 4. Spectral index maps of HB3 calculated for three frequency pairs.

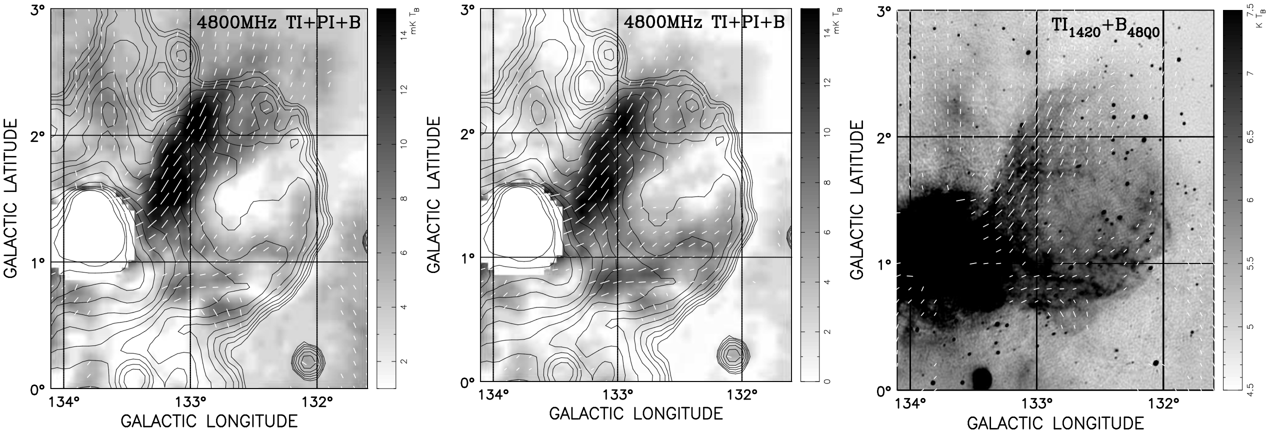

Fig. 5. Polarised emission from HB3 detected at 4800 MHz. *Left panel:* Total intensity map at 4800 MHz is displayed by contours, and the polarised intensity map is shown in grey-scale. The bars represent ($\boldsymbol{E} + 90°$), roughly indicating the magnetic field orientation. The bar length is proportional to the polarised intensity. The diffuse Galactic emission is not subtracted. *Middle panel:* Same as the *left* but diffuse Galactic polarised emission has been removed from the polarised intensity map. *Right panel:* Polarisation angles ($\boldsymbol{E} + 90°) \simeq \boldsymbol{B}$ calculated from original maps at 4800 MHz are plotted over the high-resolution 1420 MHz total intensity map (grey-scale) from the Canadian Galactic Plane Survey (Taylor et al., 2003).

Routledge, D., Dewdney, P. E., Landecker, T. L., & Vaneldik, J. F. 1991, A&A, 247, 529
Sun, X. H., Han, J. L., Reich, W., et al. 2007, A&A, 463, 993
Taylor, A. R., Gibson, S. J., Peracaula, M., et al. 2003, AJ, 125, 3145
Tian, W. W., & Leahy, D. 2005, A&A, 436, 187
Tian, W. W., & Leahy, D. A. 2006, erratum, A&A, 451, 991
Urošević, D., Pannuti, T. G., & Leahy, D. 2007, ApJ, 655, L41
Venkatesan, D., Leahy, D. A., Galas, C. M. F., Naranan, S., & Long, K. 1984, MNRAS, 208, 25P
Xiao, L., Fürst, E., Reich, W., & Han, J. L. 2008, A&A, 482, 783
Xu, Y., Reid, M. J., Zheng, X. W., & Menten, K. M. 2006, Science, 311, 54